Theoretical and Solid-State NMR Study of Acetylene Adsorption on Nano-Sized MgO

John B. Nicholas,*,† Ali A. Kheir,‡ Teng Xu,‡ Thomas R. Krawietz,‡ and James F. Haw*,‡

Contribution from the Environmental Molecular Sciences Laboratory, Pacific Northwest National Laboratory, Richland, Washington 99352, and Center for Catalysis, Department of Chemistry, Texas A&M University, College Station, Texas 77843

Received February 3, 1998. Revised Manuscript Received June 3, 1998

Abstract: We present a combined density functional theory, gauge-including atomic orbital (GIAO), in situ ^{13}C MAS NMR, and in situ infrared study of acetylene adsorption on nano-sized MgO powder. Geometries were optimized using the hybrid B3LYP exchange-correlation functional and triple-ζ basis sets. By utilizing models of the surface ranging in size from Mg_4O_4 to Mg_8O_8, we optimized geometries for a variety of surface-bound species on corner and edges sites. No stable dissociation products on the flat, (100)-like surface of an $Mg_{12}O_{12}$ cluster could be obtained theoretically, in agreement with a previous ultrahigh vacuum surface science experiment. We also present GIAO-restricted Hartree−Fock predictions of the ^{13}C chemical shifts of all species and their vibrational frequencies. The agreement between theory and experiment is outstanding. Both the theoretical and experimental results strongly support the formation of an acetylide on the MgO surface, while an alternative vinylidene species is not present. A minority species was also observed, which both theory and experiment identify as an ethoxide. This work, the first combined theoretical and in situ NMR study of chemisorption on a (nonzeolitic) metal oxide surface, suggests that this approach will be very useful for the future study of catalytic phenomena on metal oxides.

Introduction

Metal oxides with Lewis base functionality are catalysts for a number of reactions including double-bond migration, hydrogenation and dehydrogenation, dehydration, alkylation, and condensation of various functional groups. Magnesium oxide is the most widely studied basic metal oxide.[1,2] Ultrahigh vacuum (UHV) surface science experiments have contributed to the study of MgO and other basic metal oxides.[3,4] To avoid surface charging, UHV experiments make use of very thin oxide films grown epitaxially on appropriate single-crystal metal surfaces. For example, Peng and Barteau[5,6] used X-ray photoelectron spectroscopy (XPS) to study the surface species derived from several adsorbates on MgO (100) grown on Mg (0001). The strong acids formic and acetic acid dissociatively chemisorbed on annealed (i.e., near-defect-free) MgO (100), whereas the weaker acids methanol and acetylene only physisorbed on this surface and desorbed without dissociation at modest temperatures. Contrasting behavior was observed on defected surfaces prepared by argon ion sputtering; in particular, acetylene dissociatively chemisorbed on sputtered MgO. The C(1s) XPS spectrum clearly showed the formation of acetylide at 200 K, and this signal was still detectable after heating to 500 K.

The high surface area metal oxide powders used in catalysis are expected to have surfaces composed largely by the intersection of nonpolar, low-index surface planes; in the case of cubic MgO (space group *Fm*3*m*), these are the (100) plane and the other two identical planes obtained by permutation of the index. High surface area insulating powders obviously require experimental methods that differ from those used in UHV surface science. Kheir et al.[7] have recently demonstrated the NMR detection of anionic surface species formed by the dissociative chemisorption of weakly acidic molecules on microcrystalline particles of basic metal oxides. Nitromethane was observed to deprotonate to form the aci-anion on MgO and CaO, and an allylic anion formed from 2-methylpropene on ZnO and MgO. Infrared spectra of the allylic species on ZnO were also obtained and compared with those obtained in the pioneering study of Dent and Kokes.[8,9]

Theoretical chemistry is also beginning to contribute to the understanding of chemistry of basic metal oxides,[10−18] and this process has been accelerated by the availability of computationally efficient implementations of density functional theory (DFT).[19,20] Several of us have recently reported combined NMR

* Corresponding authors.
† Pacific Northwest National Laboratory.
‡ Texas A&M University.

(1) Hattori, H. *Chem. Rev.* **1995**, *95*, 537−558.
(2) Henrich, V. E.; Cox, P. A. *The Surface Science of Metal Oxides*; Cambridge University: New York, 1994.
(3) Barteau, M. A. *Chem. Rev.* **1996**, *96*, 1413−1430.
(4) Goodman, D. W. *Chem. Rev.* **1995**, *95*, 523−536.
(5) Peng, X. D.; Barteau, M. A. *Catal. Lett.* **1992**, *12*, 245−254.
(6) Peng, X. D.; Barteau, M. A. *Langmuir* **1991**, *7*, 1426−1431.
(7) Kheir, A. A.; Haw, J. F. *J. Am. Chem. Soc.* **1994**, *116*, 817−818.
(8) Dent, A. L.; Kokes, R. J. *J. Am. Chem. Soc.* **1970**, *92*, 1092−1093.
(9) Dent, A. L.; Kokes, R. J. *J. Am. Chem. Soc.* **1970**, *92*, 6709−6723.
(10) Allouche, A. *J. Phys. Chem.* **1996**, *100*, 1820−1826.
(11) Anchell, J. L.; Glendening, E. D. *J. Phys. Chem.* **1994**, *98*, 11582−11587.
(12) Anchell, J. L.; Hess, A. C. *J. Phys. Chem.* **1996**, *100*, 18317−18321.
(13) Boldyrev, A. I.; Simons, J. *J. Phys. Chem.* **1996**, *100*, 8023−8030.
(14) Ferry, D.; Hoang, P. N. M.; Suzanne, J.; Biberian, J. P.; van Hove, M. A. *Phys. Rev. Lett.* **1997**, *78*, 4237−4240.
(15) Johnson, M. A.; Stefanovich, E. V.; Truong, T. N. *J. Phys. Chem.* **1997**, *101*, 3196−3201.
(16) Langel, W.; Parrinello, M. *J. Chem. Phys.* **1995**, *103*, 3240−3252.
(17) McCarthy, M. I.; Schenter, G. K.; Scamehorn, C. A.; Nicholas, J. B. *J. Phys. Chem.* **1996**, *100*, 16989−16995.
(18) Pacchioni, G.; Ricart, J.; Illas, F. *J. Am. Chem. Soc.* **1994**, *116*, 10152−10158.

S0002-7863(98)00384-9 CCC: $15.00
Published on Web 09/23/1998

experiments and theoretical calculations probing adsorption and reaction on zeolite and metal halide solid acids.[21−23] Here we report our first combined theoretical and NMR study of chemistry on a basic metal oxide. We selected the adsorption of acetylene on MgO powders because of the previous UHV surface science study, and because the systems required to model, the adsorbed species considered presented a challenging but tractable computational objective.

We used in situ ^{13}C NMR with magic angle spinning (MAS) and FTIR spectroscopy in diffuse reflectance mode to measure spectra of the species formed by adsorption of acetylene on MgO powders. The materials examined were a microcrystalline MgO formed from a conventional $Mg(OH)_2$ gel and nanocrystalline MgO formed through the supercritical aerogel route developed by Klabunde.[24]

The theoretical part of this study utilized DFT methods to obtain optimized geometries for the various species adsorbed on MgO clusters. We used a variety of clusters to investigate the sensitivity of the results to cluster geometry. To more closely relate the experimental and theoretical results, we also performed chemical shift calculations using the gauge-including atomic orbital (GIAO) method on all of the theoretical models. In addition, predictions of the IR spectra were obtained from DFT frequency calculations.

Theoretical Details

All geometry optimizations were done using DFT[25,26] as implemented in the program Gaussian94.[27] We used the B3LYP[28,29] hybrid functional that includes a component of the exact (Hartree−Fock) exchange in a parametrized fashion.

Optimizations were done using the DFT-optimized polarized triple-ζ valence basis sets of Godbout and co-workers[30] (TZVP). Whereas the original TZVP basis set did not include Mg, for this atom, we substituted a similar polarized triple-ζ basis (TZ94) from the UniChem program library.[31] To achieve higher accuracy energetics, we did single-point calculations at the TZVP-optimized geometries using an extended basis set. This basis set, termed TZVP+, adds a diffuse s (H) or s and p (all other atoms) to the TZVP basis set. The exponents of the additional functions were obtained from an even-tempered expansion[32] of the outer functions in the standard basis set. The TZVP and TZVP+ basis sets were used with six (Cartesian) d functions.

The initial calculations were done using a cubic cluster model of MgO (Mg_4O_4). The geometry of the cube was fixed at that of the bulk (Mg−O distance = 2.106 Å), whereas the acetylene was allowed complete flexibility during the optimization. Although C_s symmetry was evident in the final geometries of many adsorption complexes, no symmetry was imposed during the optimizations. Frequency calculations were done at the B3LYP/TZVP geometries. Despite the fact that the MgO model was frozen, in every case, all frequencies were positive, including those associated with the MgO. The exception was for a transition state for acetylene dissociation, in which a strong negative frequency corresponding to the transfer of H to a surface O was obtained. The frequencies were scaled by 0.95 to account for anharmonicity when compared to experimental IR values.

Additional calculations were done using larger models of the MgO surface (Mg_6O_6 and Mg_8O_8). These calculations allowed us to explore the sensitivity of the calculated geometries and relative energetics to the size of the cluster. We were also able to investigate modes of bonding that were not possible on the smaller cluster. All the additional optimizations were also done at the B3LYP/TZVP level of theory, followed by B3LYP/TZVP+ single-point calculations. The larger models of the surface were also fixed at bulk MgO geometries. As before, all the B3LYP/TZVP frequencies of the optimized geometries were positive. One additional calculation used an even larger MgO model ($Mg_{12}O_{12}$) to represent the flat surface.

Predictions of the ^{13}C chemical shifts of the adsorbed species were obtained using the gauge-including atomic orbital[33] (GIAO) method at the restricted Hartree−Fock[34,35](RHF) level of theory. We favor the RHF-GIAO calculations over using the GIAO method within the DFT formalism, as our experience indicates the RHF-GIAO calculations are often more reliable. We prefer to use the second-order Møller−Plessett (MP2) GIAO implementation by Gauss[36] in AcesII, however, the clusters considered are much too large for that code to handle. All reported RHF-GIAO chemical shifts are reported relative to the values obtained for calculations of tetramethylsilane (TMS) at the same level of theory. Further details are given in the Appendix.

Experimental Details

Materials. We prepared the microcrystalline oxide powders as follows: MgO (Fischer Scientific ACS certified grade) was hydroxylated by mixing the respective oxide with deionized water (30 mL per gram of oxide) to form a white slurry. We slowly heated the slurry to dryness, broke it into pieces, and then ground it to a fine powder. The powder was then further dried in an oven at 373 K for 12 h. Prior to adsorption, the oxide was thermally activated to a maximum temperature of 773 K by using a multistep procedure described previously[37] and maintained at 773 K for 2 h under continuous evacuation.

We prepared nanocrystalline MgO according to the method of Klabunde.[24,38] Mg powder (Aldrich 99% pure, −50 mesh) was reacted under N_2 purge with 203 mL of anhydrous CH_3OH to form a 10% $Mg(OCH_3)_2/CH_3OH$ solution. The resultant 10% $Mg(OCH_3)_2$ (40 mL) was then added to 200 mL of toluene, followed by dropwise addition of 1.6 mL of water and stirred overnight. The resultant colloidial suspension of $Mg(OH)_2$ was placed in an autoclave, pressurized to 100 psig with dry N_2, and heated slowly to 538 K and a final pressure of ∼1400 psi. The supercritical solvent was vented to produce a fine white powder of $Mg(OH)_2$. Nanocrystalline MgO was obtained by heating the fine powder at 773 K under vacuum. BET surface area of nanocrystalline MgO, as determined by N_2 adsorption, was ca. 380 m^2 g^{-1}.

(19) Andzelm, J.; Wimmer, E. *J. Chem. Phys.* **1992**, *96*, 1280.
(20) Delley, B. *J. Chem. Phys.* **1990**, *92*, 508. DMol is sold by Biosym Technologies, San Diego, CA.
(21) Haw, J. F.; Nicholas, J. B.; Xu, T.; Beck, L. W.; Ferguson, D. B. *Acc. Chem. Res.* **1996**, *29*, 259−267.
(22) Haw, J. F.; Nicholas, J. B. In *Proceedings of the 11th Int. Congress on Catalysis*; Hightower, J. W., Delgass, W. N., Eds.; Elsevier: Amsterdam, 1996; pp 573−580.
(23) Nicholas, J. B.; Haw, J. F.; Beck, L. W.; Krawietz, T. R.; Ferguson, D. B. *J. Am. Chem. Soc.* **1995**, *117*, 12350−12351.
(24) Klabunde, K. J.; Stark, J.; Koper, O.; Mohs, C.; Park, D. G.; Decker, S.; Jiang, Y.; Lagadic, I.; Zhang, D. *J. Phys. Chem.* **1996**, *100*, 12142−12153.
(25) Andzelm, J. In *Density Functional Methods in Chemistry*; Labanowski, J., Andzelm, J., Eds.; Springer-Verlag: New York, 1991; p 155.
(26) Ziegler, T. *Chem. Rev.* **1991**, *91*, 651−667.
(27) Frisch, M. J.; Trucks, G. W.; Schlegal, H. B.; Gill, P. M. W.; Johnson, B. G.; Robb, M. A.; Cheeseman, J. R.; T. Keith; Petersson, G. A.; Montgomery, J. A.; Raghavachari, K.; Al-Laham, M. A.; Zakrzewski, V. G.; Ortiz, J. V.; Foresman, J. B.; Cioslowski, J.; Stefanov, B. B.; Nanayakkara, A.; Challacombe, M.; Peng, C. Y.; Ayala, P. Y.; Chen, W.; Wong, M. W.; Andres, J. L.; Replogle, E. S.; Gomperts, R.; Martin, R. L.; Fox, D. J.; Binkley, J. S.; Defrees, D. J.; Baker, J.; Stewart, J. P.; Head-Gordon, M.; Gonzalez, C.; Pople, J. A. *Gaussian 94*, Revision B.2; Gaussian, Inc.: Pittsburgh, PA, 1995.
(28) Becke, A. D. *J. Chem. Phys.* **1993**, *98*, 5648−5652.
(29) Lee, C.; Yang, W.; Parr, R. G. *Phys. Rev. B* **1988**, *37*, 785−789.
(30) Godbout, N.; Salahub, D. R.; Andzelm, J.; Wimmer, E. *Can. J. Chem.* **1992**, *70*, 560−571.
(31) UniChem 4.0 is distributed by Oxford Molecular, Beaverton, OR.
(32) Van Duijeneveldt, F. IBM Technical Report RJ-945, 1971.
(33) Ditchfield, R. *Mol. Phys.* **1974**, *27*, 789−807.
(34) Cheeseman, J. R.; Trucks, G. W.; Keith, T. A.; Frisch, M. J. *J. Chem. Phys.* **1996**, *104*, 5497−5509.
(35) Wolinski, K.; Hinton, J. F.; Pulay, P. *J. Am. Chem. Soc.* **1990**, *112*, 8251−8260.
(36) Gauss, J. *Chem. Phys. Lett.* **1992**, *191*, 614−620.
(37) Murray, D. K.; Chang, J.-W.; Haw, J. F. *J. Am. Chem. Soc.* **1993**, *115*, 4731−4741.
(38) Utamapanya, S.; Klabunde, K. J.; Schlup, J. R. *Chem. Mater.* **1991**, *3*, 175−181.

Acetylene-$^{13}C_1$ and -$^{13}C_2$ (99% ^{13}C) were obtained from CDN and Cambridge Isotope, respectively.

Sample Preparation for In Situ MAS NMR. All samples for the NMR experiments were prepared using the standard CAVERN device.[39] Typically, about 0.25−0.30 g of the activated catalyst was loaded into a 7.5-mm rotor inside a drybox under a nitrogen atmosphere. The rotor was then placed in the CAVERN, and the CAVERN was then transferred to a vacuum line where it was evacuated to pressures less than 5×10^{-5} Torr. Adsorbate loadings were around 0.6 mmol/g (less than 1 monolayer). All adsorptions were done at room temperature.

NMR Spectroscopy. We performed in situ ^{13}C solid-state NMR experiments with MAS on extensively modified Chemagnetics CMC-200 and Chemagnetics CMC-300 spectrometers, operating at 50.06 and 75.4 MHz, respectively. We used hexamethylbenzene (17.4 ppm) as an external chemical shift standard, and we report all chemical shifts relative to TMS. The following ^{13}C NMR experiments were performed: cross polarization (CP), contact time = 2 ms, pulse delay = 4 s, 400−1600 transients; CP with interrupted decoupling (ID), contact time = 2 ms, pulse delay = 4 s, 400−1600 transients, dipolar dephasing time of 50 μs; single-pulse excitation with decoupling (Bloch decay), pulse delay = 10 s, 400−1600 transients. Except where otherwise stated all spectra were acquired using the above parameters.

Infrared Spectroscopy. We also studied the products of acetylene on MgO by infrared spectroscopy. We designed a sample preparation method that allowed us to obtain NMR and IR spectra of identically prepared samples. Nanocrystalline MgO (0.35 g) was activated in a shallow-bed CAVERN using a mutistep temperature program with a highest activation temperature of 723 K. Acetylene-$^{13}C_2$ (200 Torr) was introduced into the shallow-bed CAVERN at 298 K and was allowed to react with MgO for 30 min at 323 K. To simplify spectral assignments for acetylide and ethoxy species, excess physisorbed acetylene was removed by extended evacuation for 60 min at 298 K. The sample was then isolated from vacuum line and was taken into a glovebox. A portion of the sample was packed into a diffuse reflectance chamber, and the chamber was sealed inside the glovebox; the rest of the sample was then packed into a 7-mm NMR rotor for ^{13}C MAS NMR measurements at 298 K. Diffuse reflectance infrared Fourier transform (DRIFT) spectra were measured on a Nicolet 510P spectrometer equipped with a MCT detector and a Spectra-Tech high-temperature/high-pressure chamber with ZnSe windows. KBr fine powders were used for acquiring background spectra. Typically 3200 scans were averaged with a resolution of 4 cm^{-1}.

Experimental Results

^{13}C MAS NMR spectra were acquired for several dozen samples of MgO prepared in various ways and then exposed to different loadings of labeled acetylene. The results obtained were not strongly sensitive to sample preparation conditions. Figure 1 reports spectra obtained immediately after preparation at 298 K for acetylene-$^{13}C_1$ on a sample of nanocrystalline MgO (Figure 1a−d) and a sample of microcrystalline MgO (Figure 1e). ^{13}C signals at 96 and 121 ppm are seen in both Bloch decay (Figure 1a) and cross polarization (Figure 1b) spectra. The definitive assignment of these signals to a corner acetylide formed on an otherwise three-coordinate cation site is made below on the basis of extensive theoretical modeling and ab initio chemical shift calculations. This assignment is also consistent with interrupted decoupling experiments; Figure 1c shows that the 121 ppm signal survives 50 μs of interrupted decoupling, as expected for a carbon without an attached proton, but the 96 ppm signal does not survive, the expected result for a static C−H group.

The 77 ppm resonance in Figure 1a−c is due to physisorbed acetylene as suggested by the observation that its relative intensity is sensitive to sample preparation conditions (e.g., capping the rotor in an overpressure of acetylene) and evidence

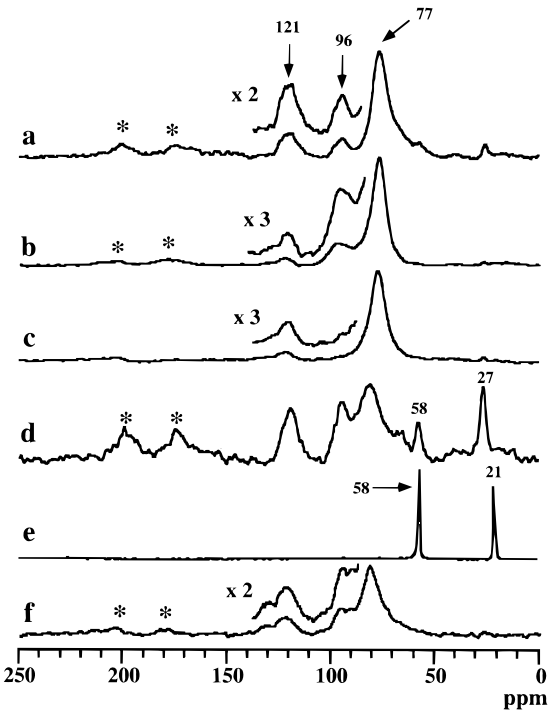

Figure 1. 50.1-MHz ^{13}C MAS NMR spectra showing the characterization of products following the reaction of acetylene-$^{13}C_1$ (CDN Isotopes) on MgO at 298 K. The loading of acetylene was 0.6 mmol/g. All spectra were acquired with 1600 transients and at 298 K. Spectra a−d are for acetylene on nanocrystalline MgO: (a) Bloch decay (BD) and pulse delay of 10 s; (b) cross polarization (CP); (c) interrupted decoupling (ID); (d) BD acquired 12 h later. (e) CP spectrum of the model compound $Mg(OCH_2CH_3)_2$. (f) BD spectrum of acetylene on microcrystalline MgO. All BD spectra were acquired with a pulse delay of 10 s, whereas CP and ID spectra were acquired with a 4-s pulse delay and a contact time of 2 ms. For the ID spectrum a dipolar dephasing period of 50 μs was used. Asterisks denote spinning side bands.

of its mobility including survival of interrupted decoupling, even at reduced temperatures. The exact chemical shift of this species is also loading dependent. Figure 1d is a Bloch decay spectrum of the above sample after it had been stored at 298 K for 12 h. Comparison of parts a and d of Figure 1 suggests that physisorbed acetylene slowly reacted at 298 K to form additional signals at 58 and 27 ppm. This reaction reduced the amount of physisorbed acetylene, and its ^{13}C chemical shift moved downfield to 80 ppm. The 58 ppm peak did not survive interrupted decoupling, but the 27 ppm resonance did (spectrum not shown). We later apply theoretical chemistry to assign these signals to an ethoxide formed on a defect site. This assignment is also supported by experimental results, including model compound studies. For example, Figure 1e is a spectrum of $Mg(OCH_2CH_3)_2$, and the ^{13}C shifts of this compound are in good (CH_3) or excellent (CH_2) agreement with the surface species. Adsorption of ethanol-*1*-^{13}C onto MgO, also produced a 58 ppm shift (not shown).

Figure 1f is a Bloch decay spectrum similar to Figure 1e except that the sample was prepared on microcrystalline MgO. The general features are similar for the two spectra with the exception that the resonances are slightly broader on the microcrystalline MgO sample. The ethoxide species also formed on the microcrystalline sample with mild heating or prolonged standing (spectra not shown).

Figure 2 shows an infrared difference spectrum of the products of acetylene-$^{13}C_2$ on nanocrystalline MgO paired with a ^{13}C NMR spectrum measured on the same sample. Since

(39) Xu, T.; Haw, J. F. *Topics Catal.* **1997**, *4*, 109−118.

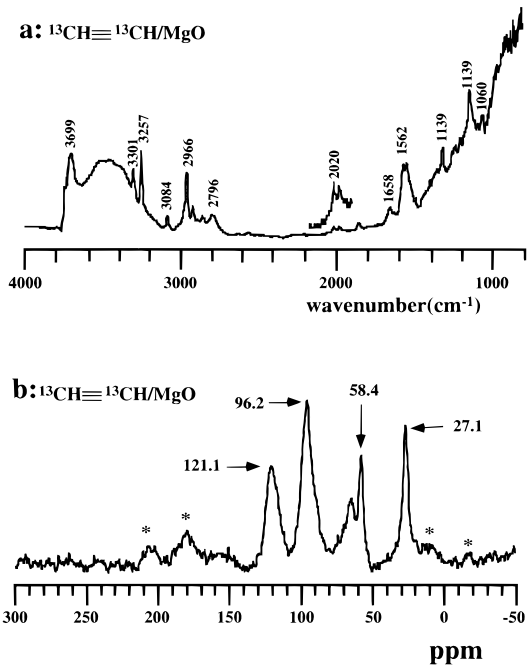

Figure 2. DRIFT difference spectrum (a) and 75.4-MHz ^{13}C MAS NMR spectrum (b) of the acetylide and ethoxy species formed from the reaction of acetylide-$^{13}C_2$ on MgO. The IR and NMR spectra were measured on samples prepared under identical conditions. See the text for detailed assignment.

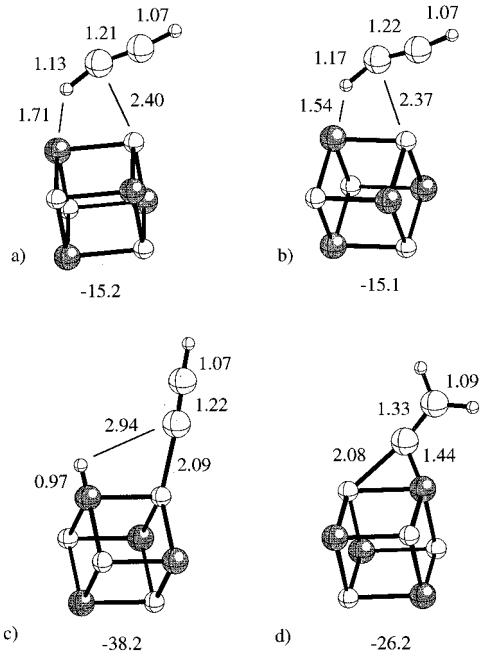

Figure 3. B3LYP/TZVP-optimized geometries for (a) physisorbed acetylene, (b) the transition state for dissociation into the acetylide, (c) the acetylide, and (d) the vinylidene on Mg_4O_4. Selected interatomic distances are in Å. Also included are the B3LYP/TZVP+//B3LYP/TZVP energies of the complexes relative to the isolated reactants.

physisorbed acetylene-$^{13}C_2$ was removed by evacuation, the NMR spectrum only shows resonances for acetylide (121 and 96 ppm) and ethoxy (58 and 27 ppm). Consistent with the NMR results, the IR spectrum shows the formation of acetylide (3257 cm^{-1} for C−H stretch and 2020 cm^{-1} for C≡C stretch) and ethoxy (2966 cm^{-1} for C−H stretch, 1060 cm^{-1} for the C−C stretch, and 1139 cm^{-1} for the C−O stretch). The assignment of the ethoxy species was verified by theoretical calculations (vide infra) and by comparison with IR spectra of model compounds, such as $Mg(OCH_2CH_3)_2$, and of ethoxy species prepared directly from the reaction of ethanol with nanocrystalline MgO (spectra not shown). The assignment of C−H modes was further verified by analogous experimentation using acetylene-d_2 (not shown).

Theoretical Results

The first goal of the theoretical study is to determine the preference for dissociation to the acetylide or vinylidene species and the spectroscopic signatures each might exhibit. While the energetics of the various dissociation pathways are clearly important, our most direct connection to the experimental data was through the prediction of ^{13}C NMR chemical shifts and IR frequencies for the possible adsorbed species. Although it was our expectation that only the acetylide would form, we did not have a means by which we could a priori dismiss the formation of the vinylidene. In the next section we focus our comparison on the experimental results for the fresh catalyst. Consideration of addition species on the aged catalyst follows.

Geometries and Energies of Binding States on Mg_4O_4. We first present the results obtained using the smallest (Mg_4O_4) cluster model. The Mg_4O_4 cluster can only be used to model adsorption on corner sites (where both Mg and O are only three-coordinate). These sites are known to be highly reactive, and we expect dissociation to form the acetylide or vinylidene species to proceed readily. We are able to identify three potential-energy minima; a physisorbed state, an acetylide, and a vinylidene (Figure 3). A transition state for the conversion of the physisorbed state to the acetylide was also obtained (the frequency corresponding to proton transfer is 269i cm^{-1})

In the physisorbed state, the H on acetylene is very close to a cluster O (1.71 Å), a distance much shorter than the sum of the van der Waals radii of the two atoms. The C of acetylene is also very close to the surface Mg (2.09 Å), indicative of the pending dissociation to form the acetylide. The C−H bond length is longer (1.13 Å) than in isolated acetylene (1.07 Å at the same level of theory), indicating a large amount of H transfer to the surface. In the transition state, both the C−H and C−Mg distance shorten slightly, whereas the O−H distance is smaller by ≈0.3 Å. In the acetylide, the H is fully transferred to the surface O. The O−H bond distance of 0.97 is consistent with other O−H bond distances at this level of theory (O−H in H_2O at B3LYP/TZVP = 0.965 Å). The Mg−C distance is somewhat longer than that of either the physisorbed or transition states. In all of the three states so far discussed, the length of the C−C triple bond (1.21−1.22 Å) and terminal C−H bond (1.07 Å) of acetylene are almost unchanged from the values in isolated acetylene (1.200 and 1.069 Å, respectively) optimized at the same level of theory. The experimental values for these two bond lengths in acetylene are 1.203 and 1.060 Å, which indicates that the accruacy of the B3LYP/TZVP optimizations is excellent.

For the vinylidene, the C is much closer to Mg than O, but the geometry indicates some stabilization from allowing the C to "bridge" the two surface atoms. Attempts at finding a geometry in which the C is associated with Mg only were unsuccessful. As expected, the C−C bond length (1.33 Å) is much longer than in the acetylide, consistent with the change from a triple to a double bond. For comparison, the C═C bond length in ethylene at B3LYP/TZVP is 1.328 Å.

The energies of the various states, reported relative to the energy of acetylene and Mg_4O_4 at infinite separation, are given in Table 1. The physisorbed state is tightly bound, being 15.7 kcal/mol lower in energy than the reactants. The transition state is only 0.1 kcal/mol higher in energy than the physisorbed state.

Table 1. Energies (kcal/mol) of the Adsorption Complexes on Mg_4O_4[a]

theory	physisorbed	transition state	acetylide	vinylidene
B3LYP/TZVP	−15.7	−15.6	−39.2	−27.1
B3LYP/TZVP+// B3LYP/TZVP	−15.2	−15.1	−38.2	−26.2

[a] All values are reported relative to the sum of the energies of isolated acetylene (optimized) and Mg_4O_4 (frozen at bulk geometry).

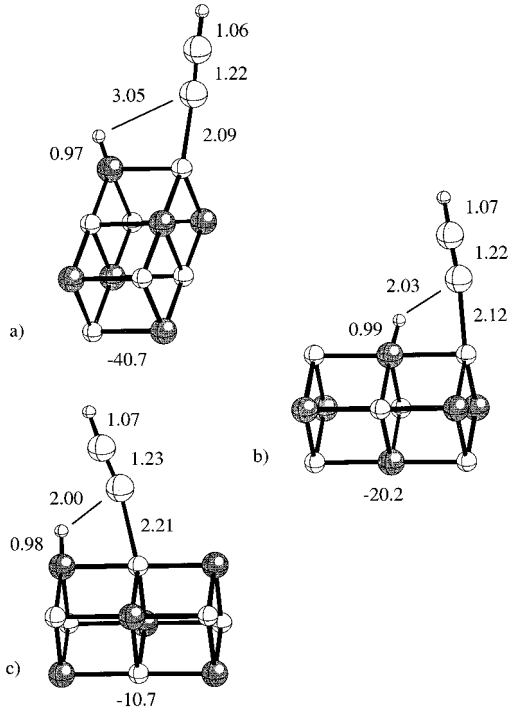

Figure 4. B3LYP/TZVP-optimized geometries for the acetylide on Mg_6O_6. Selected interatomic distances are in Å. Also included are the B3LYP/TZVP+//B3LYP/TZVP energies of the complexes relative to the isolated reactants.

It seems likely that the physisorbed state is an artifact of the calculation. Even if did form, the very low barrier to conversion to the acetylide would indicate that the physisorbed state would not be observed experimentally. The acetylide is the most stable species formed, being 39.2 kcal/mol lower in energy than the reactants. The vinylidene is ≈12 kcal/mol less stable.

Using the larger basis set (TZVP+) at the B3LYP/TZVP geometry, the adsorption energy decreases to 15.2 kcal/mol. For the acetylide, the B3LYP/TZVP+ single-point calculation lowers the binding energy to −38.2 kcal/mol. Finally, the B3LYP/TZVP+ single-point energy indicates that the vinylidene is ≈1.0 kcal/mol less strongly bound than the B3LYP/TZVP calculation predicts. The small decreases in all the relative energies with the larger basis set are consistent with a reduction in the basis set superposition error.

Geometries and Energies of Binding States on Mg_6O_6. In Figure 4 we show the B3LYP/TZVP-optimized geometries of three possible acetylides formed on an Mg_6O_6 cluster. The geometry of the acetylide formed on the end of the cluster, where both Mg and O are 3-fold coordinate, is very similar to that obtained on the Mg_4O_4 model; all bond distances agree within less than 0.005 Å. If we consider dissociation on sites in which Mg is three-coordinate and O is four-coordinate, a slightly different geometry is obtained. Both the O−H and Mg−C bond lengths are lengthened, suggesting a weaker bonding to the surface. In addition, the dissociated H is much closer to the nearest C (2.03 Å) than in either of the structures in which both

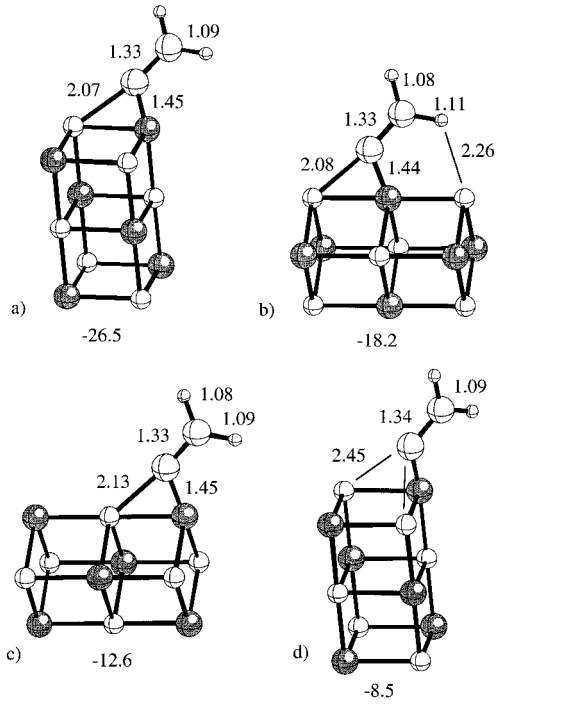

Figure 5. B3LYP/TZVP-optimized geometries for the vinylidene on Mg_6O_6. Selected interatomic distances are in Å. Also included are the B3LYP/TZVP+//B3LYP/TZVP energies of the complexes relative to the isolated reactants.

surface sites are 3-fold coordinate (2.94 Å on Mg_4O_4 and 3.05 Å on Mg_6O_6). This close contact is suggestive of a much lesser degree of dissociation on the surface. In the case in which O is three-coordinate and Mg is four-coordinate, we also obtain a geometry in which the acetylide appears less fully dissociated on the surface. Both O−H and Mg−C bond distances are longer than when both surface atoms are three-coordinate, and the H−C nonbonded distance is notably shortened (2.00 Å). The Mg−C distance (2.2 Å), in particular, is much longer than when C is bonded to three-coordinate Mg (2.09 Å).

We have obtained four stable potential energy minima for a vinylidene on the corner sites of Mg_6O_6 (Figure 5). As was the case for the acetylide, if both O and Mg are three-coordinate, the optimized geometry is very similar to that obtained on Mg_4O_4. Bond distances are the same within 0.005 Å. If we adsorb the molecule on an edge of the cluster, in which O is three-coordinate and Mg is four-coordinate, there is little change in the geometry. However, one of the H of the vinylidene is closely associated with a different surface O. The C−H bond is also slightly lengthened. The geometry of this species suggests that transfer of a proton to the surface, and thus the formation of a surface acetylide, might occur readily. We did not attempt to locate a transition state for this transformation. Two additional states in which C is bonded to three-coordinate Mg were located. In one of these states C bridges Mg and a single (four-coordinate) O as it does in all the other optimized geometries, and the resulting structure is very similar to the cases in which both surface atoms are three-coordinate. In the other state, C bridges Mg and two (three-coordinate) O, at a much greater distance (2.45 Å versus ≈2.1 Å in all the other cases).

The B3LYP/TZVP+ relative energy of the acetylide bound to the two three-coordinate sites on Mg_6O_6 is −40.7 kcal/mol, very similar to the value of −38.2 kcal/mol obtained with a similar geometry on Mg_4O_4. The structure in which O is three-coordinate whereas Mg is four-coordinate is much less stable,

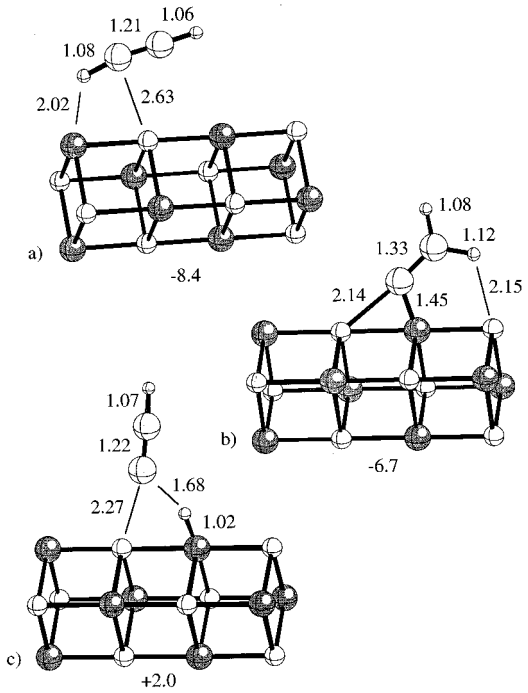

Figure 6. B3LYP/TZVP-optimized geometries for (a) physisorbed acetylene, (b) the vinylidene, and (c) the acetylide on Mg_8O_8. Selected interatomic distances are in Å. Also included are the B3LYP/TZVP+// B3LYP/TZVP energies of the complexes relative to the isolated reactants.

being 20.2 kcal/mol lower than the isolated reactants. Finally, when acetylide is bound to three-coordinate Mg and four-coordinate O, the binding energy is only −10.7 kcal/mol.

Similar trends in relative energy are seen for the vinylidene species. The B3LYP/TZVP+ binding energy for vinylidene bound to two three-coordinate surface atoms is −26.5 kcal/mol, 0.3 kcal/mol more tightly bound than the analogous species on Mg_4O_4. When the vinylidene is associated with a four-coordinate Mg and three-coordinate O, the binding energy is decreased to −18.2 kcal/mol. The binding energy is further lowered to −12.6 kcal/mol on three-coordinate Mg and four-coordinate O. Finally, the state in which the vinylidene C bridges two four-coordinate surface atoms is bound by only 8.5 kcal/mol.

Geometries and Energies of Binding States on Mg_8O_8. Considering the very similar geometries and relative energies obtained for similar binding states on the Mg_4O_4 and Mg_6O_6 clusters, we felt it unnecessary to duplicate these optimizations on a still larger cluster. However, on Mg_8O_8, we were able to investigate binding modes not possible on Mg_4O_4 and Mg_6O_6. In contrast to the smaller clusters in which adjacent atoms are either both three-coordinate or one is three-coordinate and the other is four-coordinate, in Mg_8O_8, there are "edge" sites at which adjacent atoms are both four-coordinate. In light of the trends on binding energies with the degree of coordination mentioned earlier, we expect that, when neither surface atom is three-coordinate, the binding energy will be further reduced from what we have presented so far.

The only stable geometry we were able to find for physisorption of acetylene is that illustrated in Figure 6, in which a H of acetylene is coordinated to a three-coordinate O on the end of the cluster. In comparison to the other geometries for physisorption presented earlier in Figures 3 and 4, in this case, the interaction between the cluster and acetylene is much weaker. The O−H interatomic distance has lengthened by 0.3 Å, and the Mg−C distance has increased by 0.2 Å. We have not attempted to locate the transition state between this geometry and the acetylide.

Also shown in Figure 6 is the optimized geometry for the acetylide on an edge site. Although this unusual geometry is a stable minimum (and not a transition state), it is clear that only partial dissociation has occurred. In contrast to the other acetylide geometries, the Mg−C distance is 0.2 Å longer. In addition, the C remains in very close contact with the H on the surface (1.68 Å), and the O−H bond distance is slightly longer than in the other cases.

There is also a stable geometry for the vinylidene bound to four-coordinate O and Mg. As was the case for the optimization on the Mg_6O_6 cluster, one of the H of the vinylidene is in close proximity to a surface O. The bond distance between the vinylidene and the cluster, and the internal coordinates of the vinylidene, are very similar to those obtained on the smaller clusters.

The physisorbed acetylene has a binding energy of −8.4 kcal/mol, approximately half of what it was on the Mg_4O_4 cluster. The weaker binding energy is consistent with the longer distances between the acetylene and the cluster atoms. The vinylidene species is weakly bound to the surface, 6.7 kcal/mol lower in energy than the isolated molecule and cluster. The binding energy is between 2 and 22 kcal/mol less on the edge site than similar structures on the Mg_4O_4 and Mg_8O_8 clusters. Finally, the energy of the acetylide on the edge site is 2.0 kcal/mol *higher* than the isolated molecules. As stated earlier, frequency calculations verify that this state is a minimum on the potential energy surface. However, it is clear from the relative energetics that this state would have no appreciable lifetime.

The above results further confirm prior observations that the corner sites on MgO are highly reactive, and the reactivity sharply decreases with the increased coordination of the surface atoms. The stronger binding (and by implication higher reactivity) of the less-coordinated sites as demonstrated here has been reported in theoretical studies of other molecules adsorbed on MgO.[11−13] As a final test of this trend, we did one optimization of a large cluster ($Mg_{12}O_{12}$) which provides sites in which both surface atoms are five-coordinate. Starting with a geometry for the adsorbed acetylide similar to that obtained on the Mg_4O_4 and Mg_6O_6 clusters, we were not able to optimize a stable geometry in which the acetylide was bound to the five-coordinate atoms of the flat surface. In fact, the acetylide in our initial geometry "desorbed" from the flat surface during the course of the optimization and reformed acetylene. This theoretical finding is in complete agreement with the experimental observation of Barteau that acetylene desorbs from defect-free MgO (100) without dissociative chemisorption.[5,6]

GIAO-RHF ^{13}C Chemical Shifts. In a recent series of papers, we have been successful in comparing experimental and theoretical ^{13}C chemical shifts for species encountered in acid catalysis.[21−23,40] In the specific case of carbenium ions, we found that highly accurate results generally required computationally expensive treatment of electron correlation at the GIAO-MP2 level. We were pleased to find that the GIAO-RHF level appeared to be sufficient for the species encountered in the reactions of acetylene on MgO. The appropriateness of the basis set is another important consideration in chemical shift calculations. We carefully evaluated the effects of basis set size and flexibility for one of the species considered in this study. The details of this investigation are given in the Appendix.

(40) Nicholas, J. B.; Xu, T.; Barich, D. H.; Torres, P. D.; Haw, J. F. *J. Am. Chem. Soc.* **1996**, *118*, 4202−4203.

Table 2. GIAO-RHF ^{13}C Chemical Shifts (ppm) for the Two Carbons of the Acetylide on Various MgO Clusters[a]

MgO model	coordination		chemical shift	
	Mg	O	−C−	−C−H
Mg_4O_4	3	3	120.9	101.0
Mg_6O_6	3	3	120.6	100.8
Mg_6O_6	3	4	119.2	107.3
Mg_6O_6	4	4	136.8	100.6
Mg_8O_8	4	4	123.3	106.7
exptl			120	96

[a] The coordinations of the surface Mg and O to which the acetylide is bound are also shown.

Table 3. GIAO-RHF ^{13}C Chemical Shifts (ppm) for the Two Carbons of the Vinylidene on Various MgO Clusters[a]

MgO model	coordination		chemical shift	
	Mg	O	−C−	$-CH_2$
Mg_4O_4	3	3	233.1	103.7
Mg_6O_6	3	3	219.9	105.4
Mg_6O_6	3	4	226.0	93.6
Mg_6O_6	4	4	233.5	102.3
Mg_8O_8	4	4	238.2	90.2

[a] The coordinations of the surface Mg and O to which the acetylide is bound are also shown.

As noted above, the experimental peaks in the ^{13}C NMR spectra which we believe can be attributed to the acetylide are at 96 and 120 ppm. In Table 2, we show the GIAO-RHF ^{13}C chemical shifts for all the acetylide species studied. The theoretical values for the acetylide on the corner sites of either Mg_4O_4 or Mg_6O_6 are in excellent agreement with the experimental values. As noted above, these are the lowest energy acetylide species. The agreement with the acetylide bound to three-coordinate Mg and four-coordinate O is much less satisfying. Although the value for the surface-bound C is excellent, the terminal C is predicted to be almost 11 ppm downfield compared to experiment. Conversely, for the species bound to four-coordinate Mg and three-coordinate O, it is the surface-bound C that is shifted substantially downfield, while the agreement for the terminal C is similar to that obtained on the corner sites. Finally, the values for the carbons on the acetylide bound to the edge of Mg_8O_8 are both somewhat downfield from experiment.

The chemical shifts for the vinylidene, presented in Table 3, are much different. On Mg_4O_4, the calculated values are 233.1 and 103.7 ppm. The vinylidene bound to the corner sites on Mg_6O_6 gives values of 219.9 and 105.4 ppm. For all the clusters considered, the theoretical values for the terminal C are in the range of peaks observed experimentally. However, there are no experimental NMR peaks in the range predicted for the surface-bound C (219.9−238.2 ppm). The disagreement between the theoretical predictions for the vinylidene ^{13}C chemical shifts and the experimental spectra casts doubt on the existence of the vinylidene under the experimental conditions employed in this investigation.

Structures and Chemical Shifts for Ethoxy Species. Both the NMR and infrared (vide infra) experiments provided strong evidence for a second chemisorbed species on MgO powders, and this species has familiar spectroscopic signatures commonly assigned to ethoxy (CH_3CH_2O-) groups. For example, Figure 1 shows that ^{13}C NMR signals develop at 58 and 27 ppm when a sample of acetylene on nanosize MgO powder is maintained at 298 K for several hours. We reproduced this observation many times and also determined that this species formed more rapidly when the sample was heated slightly above 298 K. The intensities of these signals were in all cases much less than those of the peaks assigned to acetylide. The result in Figure 1d, in which the integrated intensities of the ethoxy signals are ca. one-third those of the acetylide signals, is typical for complete reaction at 298 K or slightly higher.

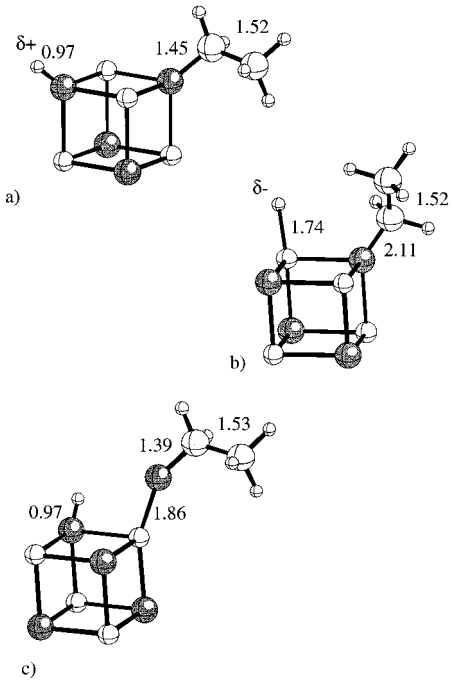

Figure 7. B3LYP/TZVP-optimized geometries for (a) surface ethoxy, (b) an alternate surface ethoxy, and (c) a dangling ethoxy on Mg_4O_4. Selected interatomic distances are in Å. Also included are the B3LYP/TZVP+//B3LYP/TZVP energies of the complexes relative to the isolated reactants.

We optimized two models of the ethoxy species which have a C_2H_5 group bound directly to a lattice O. We first consider that the C_2H_5 has a partial negative charge, with $H^{\delta+}$ bound to another lattice O to balance the charge. The B3LYP/TZVP geometry of this complex is shown in Figure 7a. We term this a "surface" ethoxy as C is bonded to a lattice O. From this single geometry we cannot calculate the overall thermodynamics of the reaction from acetylene. However, if we consider this complex to formed directly from ethane, it is 9.1 kcal/mol lower in energy than the isolated reactants. An alternative possibility is that C_2H_5 binds to surface O with a partial positive charge, with $H^{\delta-}$ bound to Mg to balance charge. The optimized geometry of this species is also shown in Figure 7b. In this case, the bond between C and the surface O is much longer (2.11 Å) than in the other surface ethoxy. Interestingly, this geometry is somewhat more stable relative to Mg_4O_4 and ethane than the first ethoxy presented, being 10.7 kcal/mol lower in energy than the reactants. For completeness, we also considered the possibility that the ethoxy forms on a surface hydroxyl, giving a "dangling" ethoxy such as that shown in Figure 7c. Formation of the species directly from ethanol is predicted to be exothermic by 50.7 kcal/mol.

The chemical shifts of the first "surface" ethoxy are 19.3 and 49.1 ppm, in reasonable but not excellent agreement with the experimental data. The chemical shifts of the other surface ethoxy are 23.8 and 55.1 ppm, giving a better agreement. The chemical shifts for the dangling ethoxy are 24.7 and 57.1 ppm, in excellent agreement with the experimental chemical shifts. While the theoretical results so far obtained cannot determine the full energetics for formation of these species on the surface, nor unambiguously differentiate between surface and dangling

Table 4. Vibration Frequencies (ν, cm^{-1}) and Intensities (I, kM/mol) of the Acetylide on Various MgO Clusters[a]

	Mg_4O_4 3/3		Mg_6O_6 3/3		Mg_6O_6 3/4		Mg_6O_6 4/3		Mg_8O_8 4/4		expt
assignment	ν	I	ν	I	ν	I	ν	I	ν	I	ν
O−H	3627.0	59.0	3634.4	70.2	3276.7	701.8	3331.9	601.6	2581.0	1915.5	3546
C−H	3274.4	24.3	3273.6	24.4	3339.8	31.7	3261.4	20.2	3266.5	25.6	3262
C≡C	1944.4	14.9	1945.7	14.9	1997.6	8.1	1907.1	14.4	1924.4	14.5	1898
O−H					1248.3	188.8	831		1149.9	235.1	1234

[a] Only frequencies above 1000 cm^{-1} are reported. The coordinations of the surface Mg and O to which the acetylide is bound are also shown. Theoretical frequencies are scaled by 0.95.

Table 5. Vibration Frequencies (ν, cm^{-1}) and Intensities (I, kM/mol) of the Vinylidene on Various MgO Clusters[a]

	Mg_4O_4 3/3		Mg_6O_6 3/3		Mg_6O_6 3/4		Mg_6O_6 4/3		Mg_8O_8 4/4	
assignment	ν	I	ν	I	ν	I	ν	I	ν	I
H−C	3040.7	8.2	3040.7	9.0	3040.7	0.7	3040.7	11.6	3040.7	0.3
H−C	2928.9	23.7	2930.8	23.3	2660.1	252.1	2908.5	50.9	2590.6	337.1
C═C, H−C−H	1563.8	137.8	1564.7	122.5	1552.5	75.7	1549.5	140.5	1538.5	63.7
H−C−H	1313.5	20.7	1313.8	16.6	1334.9	35.7	1304.4	31.8	1336.1	50.3
H−C−H	987.6	3.6	992.4	2.3	972.3	11.9	974.1	24.9	987.8	27.7

[a] Only frequencies above 1000 cm^{-1} are reported. The coordinations of the surface Mg and O to which the vinylidene is bound are also shown. Theoretical frequencies are scaled by 0.95.

ethoxy, it is clear that some form of ethoxy was present and was detected by the NMR experiment.

IR Frequencies for the Acetylide, Vinylidene, and Ethoxy. In addition to the distinct ^{13}C chemical shifts, the acetylide, vinylidene, and ethoxy should exhibit different vibrational frequencies. Table 4 gives the theoretical frequencies for modes above ≈1000 cm^{-1} for all the acetylide models. On the Mg_4O_4 model, the mode at 3627.0 cm^{-1} corresponds to the O−H stretch, the mode at 3274.4 cm^{-1} is the C−H stretch, and the 1944.4 cm^{-1} mode is the C≡C stretch. The acetylide on the corner sites of Mg_6O_6 gives almost the same frequencies, as expected for such similar geometries. Binding of the acetylide to sites of higher coordination causes shifts in some of the predicted frequencies. For example, in the complex with acetylide edge-bound to three-coordinate Mg and four-coordinate O, the O−H stretch is at 3276.7 cm^{-1} and a frequency corresponding to an O−H wag appears at 1248.3 cm^{-1}. The C≡C stretch frequency is raised slightly, as is that of the C−H stretch. Inspection of the optimized geometry of this complex explains the frequency shifts, as the H on the O is closely associated with one of the acetylide C, and the O−H bond length has increased by 0.02 Å. When the acetylide is bound to four-coordinate Mg and three-coordinate O, the O−H stretch is also shifted to lower wavenumbers.

For the acetylide bound to the corner sites, the agreement between the predicted and observed frequencies is excellent. In the experimental IR spectra, a band at 3699 cm^{-1} is commonly attributed to the O−H stretch. The peak at 3257 cm^{-1} likely corresponds to the C−H stretch. The very weak band due to the C≡C stretch is seen at 2020 cm^{-1}. The largest error is for the O−H stretch (≈72 cm^{-1}). The relative intensities of the three highest frequencies are also in qualitative agreement with the experimental measurements. The agreement between the experimental values and the theoretical frequencies for the acetylide bound on the edge of Mg_8O_8 are very poor. The O−H stretch of this species is shifted to much lower wavenumbers than in the other complexes (2581 cm^{-1}). There is no strong peak in the experimental spectra in this vicinity. The poor agreement is not surprising considering the high relative energy and unusual geometry of this complex.

In Table 5, we present similar IR data for the various vinylidene complexes. The calculation of vinylidene on Mg_4O_4 predicts C−H stretch modes in the vicinity of 3040.7 and 2928.9 cm^{-1}. The highest frequency mode is unaffected by changes in cluster size, while the other C−H stretch is greatly perturbed when the vinylidene is bound to three-coordinate Mg and four-coordinate O and when bound to the edge site on Mg_8O_8. Inspection of the geometries of these complexes explains the frequency shift, as in both cases one of the vinylidene H is closely coordinated to a surface Mg and the associated C−H bond is significantly lengthened. The frequency of the C═C bond is relatively constant for all complexes, as are the modes associated with H−C−H bends. The theoretical frequencies may have corresponding peaks in the experimental spectra. There is some indication of C−H stretches at 3084 and 2966 cm^{-1} and what could be a H−C−H bend at 1314 cm^{-1} in the experimental IR. Most notably, there is an indication of a strong band at ≈1550 cm^{-1}, which theory predicts should be apparent in the experimental IR spectra if the C═C bond were present. Whereas the frequencies corresponding to C−H stretches and H−C−H bends are also be attributed to the ethoxy species (see below), the strong band ≈1550 cm^{-1} cannot. Considering that there was no experimental or theoretical NMR evidence for the vinylidene, alternate explanations were sought. These will be discussed later.

The theoretical frequencies of the various ethoxy species considered are given in Table 6. Once again, theory predicts bands due to O−H stretches to appear at 3562.8−3598.5 cm^{-1}. A number of bands associated with the C−H stretches should appear between 2938 and 2762 cm^{-1}. Which of these bands is the most intense depends on which model of the ethoxy we use. For the surface ethoxy with H on O, this band is at 2927.7 cm^{-1}. When H is bound to Mg, the strongest band is predicted to appear at 2839.2 cm^{-1}, whereas the dangling ethoxy model suggest the strongest peak will appear at 2762.6 cm^{-1}. Generally weak peaks associated with C−H bends are predicted just above 1400 cm^{-1}. The C−C stretch frequencies are insensitive to the model used and are predicted to be in the narrow ranges of 1330−1340 and 1024−1051 cm^{-1}. Other generally weak frequencies also associated with the C−C stretch are predicted between those bands. Finally, the models give a strong peak due to the C−O stretch at 999.7 to 1139.2 cm^{-1}.

The experimental IR spectrum shows evidence of most of the frequencies predicted by the theoretical calculations. As noted before, peaks that can be attributed to O−H stretches are seen at 3699 cm^{-1}. A strong peak at 2966 cm^{-1} and several

Table 6. Vibration Frequencies (ν, cm^{-1}) and Intensities (I, kM/mol) of the Various Ethoxy Species on Mg_4O_4[a]

	C(O), H(O)		C(O), H(Mg)		C(O−Mg), H(O)	
assignment	ν	I	ν	I	ν	I
O−H (str)	3598.5	43.2			3562.8	129.1
C−H (str)	2938.0	18.7	2949.2	13.4	2919.7	38.6
C−H (str)	2927.7	37.7	2915.7	31.2	2914.0	58.9
C−H (str)	2894.2	5.3	2900.4	4.0	2850.9	25.6
C−H (str)	2864.6	12.4	2839.2	65.8	2769.3	73.1
C−H (str)	2861.5	14.6	2818.2	35.5	2762.6	170.6
C−H (bend)	1442.7	2.2	1432.7	4.4	1441.8	3.5
C−H (bend)	1418.4	6.3	1421.6	45.1	1419.5	2.7
C−H (bend)	1408.9	35.2	1410.9	30.9	1408.2	7.7
Mg−H (str)			1408.1	203.4		
C−C (str)	1339.9	61.1	1340.9	30.5	1333.0	46.2
C−C (str)	1323.1	0.1	1322.6	2.5	1314.3	5.8
C−C (str)	1247.2	2.8	1251.5	2.9	1239.8	0.3
C−C (str)	1108.5	1.7	1113.3	2.9	1114.8	1.5
C−C (str)	1051.0	24.2	1054.0	28.4	1024.0	46.8
C−O (str)	999.7	112.5	1004.3	140.2	1138.2	308.3

[a] Only frequencies above 1000 cm^{-1} are reported. Theoretical frequencies are scaled by 0.95.

weaker peaks at lower wavenumber (2916, 2861, and 2796 cm^{-1}) are likely due to C−H stretches. There is little indication of C−H bends in the 1400 cm^{-1} range. A stronger peak which could be attributed to the C−C bond stretch is seen in the experimental spectra at 1314 cm^{-1}, corresponding to the theoretical prediction at ≈1330 cm^{-1}. Another experimental C−C band at 1060 cm^{-1} may also correspond to the theoretical frequencies at ≈1050 cm^{-1}. Last, the C−O bond stretch can be seen in the experimental spectra at 1139 cm^{-1}, which theory indicates should fall in the range 999.7−1139.2 cm^{-1}. Given the above interpretation of the theoretical data, the agreement with the experimental frequencies is again quite good.

We now consider the possible explanations for the evidence of the vinylidene in the experimental data. The bands associated with C−H stretches and H−C−H bends in the vinylidene may also be due to the presence of the ethoxy species. The bands expected at ≈1300 cm^{-1} for the vinylidene H−C−H bends may also be mistaken for those of the C−C stretch in the ethoxy. However, the strong C═C peak predicted by the theoretical calculations, and seen in the IR, cannot be so easily explained. Neither the acetylide nor the ethoxy are predicted to have intense peaks in this region. However, the IR spectra (not shown) of the activated catalyst prior to adsorption has peaks at 1562 and 1539 cm^{-1} identical to those evident in Figure 2. We therefore conclude these peaks are due to carbonate species, which are well know to be present on MgO, and do not support the existence of the vinylidene. The alternate explanation for the presence of peaks that may be due to the vinylidene does not in itself rule out the presence of vinylidenes under the experimental conditions. However, it does show that a reasonable interpretation of the IR spectra that is consistent with the absence of the vinylidene in the NMR data can be made.

Summary and Conclusion

We have presented the first report in which in situ NMR and theoretical chemistry have been combined to study chemisorption on a metal oxide. The overall agreement between the theoretical and experimental results obtained by both ^{13}C NMR and infrared spectroscopy is outstanding. It is clear that acetylene dissociatively chemisorbs to form acetylide bound to magnesium. Corner acetylides formed on three-coordinate sites are energetically more stable than analogous species on a four-coordinate edge sites. The predicted spectroscopic properties of the former species are in slightly better agreement with experiment than those of the latter. However, our results also show that edge acetylides are also thermodynamically stable to dissociation, and at the relatively low temperatures used in the experimental work, edge and corner acetylides might form under kinetic control and not equilibrate. Theoretical calculations show that dissociative chemisorption of acetylene cannot occur on the five-coordinate sites of nondefected MgO (100), in agreement with previous UHV experiments by Barteau.

The formation of acetylides with formal anionic charges on strongly basic surfaces is not surprising, but formally neutral vinylidenes form on many surfaces, and we had no a priori reason for excluding their formation here as well. We can now confidently state that neither the NMR nor the infrared results provide any evidence for vinylidene species forming from acetylene on MgO powders, and the substantial energetic preference for acetylide formation shown by the theoretical studies supports this result.

We presented strong experimental evidence for the formation of ethoxide as a minority species (ca. 25%) in the presence of acetylide on MgO powders. Theoretical calculations suggested that our spectroscopic assignments were correct. Further evidence for this assignment includes comparison of the infrared frequencies with those previously observed in a study of ethanol adsorption on MgO surfaces.[41]

Several aspects of the theoretical work deserve special mention. The cluster models used in this study do not include long-range interactions, and we did not allow relaxation of the surface atoms upon chemisorption. In addition, although we were able to use accurate functionals and a triple-ζ basis set, the size of the clusters prohibited the prediction of GIAO chemical shifts beyond the RHF level of theory. Yet, the theoretical calculations reproduced the important features of the observed chemistry and provided essentially quantitative agreement between theoretical and experimental spectroscopic observables. Using similar computational techniques, we have been able to achieve equally good agreement between theoretical and experimental results for numerous aspects of zeolite chemistry.[21−23,40,42] If the accuracy of the theoretical calculations reported here can be obtained with other surfaces and adsorbates, the interpretation of metal oxide chemistry will be greatly facilitated. In fact, the synergistic application of theoretical methods and in situ spectroscopy to chemisorption on basic metal oxides appears to be even more promising than it did at a corresponding stage in the study of zeolite solid acids.

Acknowledgment. J.B.N. is funded by the Department of Energy (DOE) Office of Energy Research. Computer resources were provided by the Scientific Computing Staff, Office of Energy Research, at the National Energy Research Supercomputer Center (NERSC), Berkeley, CA, and by the National Center for Supercomputing Applications (NCSA), Urbana, IL. Pacific Northwest National Laboratory is a multipurpose national laboratory operated by Battelle Memorial Institute for the U.S. Department of Energy under Contract DE-AC06-76RLO 1830. Work at Texas A&M University on this project was supported by the National Science Foundation (CHE-9528959).

Appendix: Sensitivity of Theoretical ^{13}C Chemical Shifts to the Basis Set

We did an extensive series of calculations to test the sensitivity of the theoretical chemical shifts to the size of the

(41) Spitz, R. N.; Barton, J. E.; Barteau, M. A.; Staley, R. H.; Sleight, A. W. *J. Phys. Chem.* **1986**, *90*, 4067−4075.

Table 7. GIAO-RHF ^{13}C Chemical Shifts for the Two Carbons of the Acetylide−Mg_4O_4 Complex as a Function of Pople Basis Set[a]

basis set			no. of	chemical shift (ppm)	
C_2H_2	MgO	Mg_3O_3	functions	−C−	−C−H
6-311+G*	6-311+G*	6-311+G*	258	−1.3	3.8
6-311+G*	6-311G*	6-311G*	226	−0.9	3.8
6-311+G*	6-31G*	6-31G*	178	−0.9	3.8
6-311+G*	6-31+G*	6-31G	156	−0.9	3.9
6-311+G*	6-31G*	6-31G	148	−0.9	3.8
6-311+G*	6-31G	6-31G	138	−1.1	4.5
6-311G*	6-311+G*	6-311+G*	250	−4.4	1.1
6-311G*	6-311G*	6-311G*	218	−4.5	1.6
6-311G*	6-31G*	6-31G*	170	−5.6	2.1
6-311G*	6-31+G*	6-31G	148	−3.9	3.2
6-311G*	6-31G*	6-31G	140	−5.4	2.1
6-311G*	6-31G	6-31G	130	−5.9	2.0
6-31+G*	6-31+G*	6-31+G*	200	−10.6	−5.4
6-31+G*	6-31+G*	6-31G*	176	−10.5	−5.3
6-31+G*	6-31G*	6-31G*	168	−10.1	−5.7
6-31+G*	6-31G*	6-31G	138	−9.9	−5.7
6-31+G*	6-31G	6-31G	128	−12.6	−6.3

[a] Basis sets are specified for the acetylide, the Mg and O to which the acetylide is bound, and the remaining atoms of the cluster. The total number of basis functions is given. Chemical shifts are reported as a deviation from the experimental values (δ theoretical − δ experimental).

basis set. Using the B3LYP/TZVP-optimized geometry of the acetylide bound to the Mg_4O_4 cluster, we first obtained the GIAO-RHF chemical shifts using a range of Pople basis sets. The Pople-style basis sets included the double-ζ 6-31G basis set with and without polarization (*)[43,44] and diffuse (+)[45] functions on H or heavy atoms, as well as the approximate[46] triple-ζ 6-311G basis set[47] with similar augmentation. We considered the adsorption complex to consist of three regions: the two H and C of the acetylide (region 1), the Mg and O to which the acetylide is bound (region 2), and the remaining three Mg and O (region 3). Different basis sets are used in each region to determine the sensitivity of the NMR data to basis set size. We were particularly interested in whether a smaller basis set could be used on atoms of the cluster more distant from the carbons of interest, without a sacrifice in accuracy. The results are presented in Table 7. All values are adjusted to those of TMS calculated at the same level of theory.

If 6-31+G* is used on region 1, the difference between the theoretical and experimental values for the C bound to the surface is approximately 10 ppm. The C shifts are relatively insensitive to the basis sets used on the atoms in the other regions, although there does appear to be a slight increase in accuracy for the terminal C as more flexible basis sets are used in regions 2 and 3.

There is considerable evidence in the literature that basis sets of triple-ζ quality or better are needed to obtain accurate theoretical NMR data for neutral or positively charged organic species. We thus also did a number of calculations in which the approximate triple-ζ basis set 6-311G* was used in region 1, while other basis sets were used on the remaining regions. The 6-311G* basis set gives better agreement with the experimental values for both carbons, reducing the error by about half.

Table 8. GIAO-RHF ^{13}C Chemical Shifts for the Two Carbons of the Acetylide−Mg_4O_4 Complex as a Function of Schafer−Ahlrichs Basis Set[a]

basis set				no. of	chemical shift (ppm)	
C_2	H_2	MgO	Mg_3O_3	functions	−C−	−C−H
tzplarge+	tzplarge	tzp	tzp	244	0.89	5.02
tzplarge+	tzplarge	tzp	tzp	236	−0.16	4.19
tzplarge+	tzp	tzp	tzp	236	−0.31	4.48
tzplarge+	tzp	tzp	dzp	197	−0.10	4.31
tzplarge+	tzp	dzp	dzp	184	−2.34	5.01
tzp+	tzp+	tzp	tzp	244	0.09	5.52
tzp+	tzp	tzp	tzp	242	0.23	5.49
tzp+	tzp	tzp	dzp	203	0.58	5.36
tzp+	tzp	dzp	dzp	190	−0.32	5.85
tzp	tzp	tzp	tzp	234	−2.37	4.10
tzp	tzp	tzp	dzp	195	−2.30	3.82
tzp	tzp	dzp	dzp	182	−4.29	4.72

[a] Basis sets are specified for the acetylide C, acetylide H, the Mg and O to which the acetylide is bound, and the remaining atoms of the cluster. The total number of basis functions is given. Chemical shifts are reported as a deviation from the experimental values (δ theoretical − δ experimental).

Once again, the theoretical values show only a slight tendency toward better agreement with experiment with increases in basis set flexibility in regions 2 and 3.

Our last set of results for the Pople basis sets were obtained using 6-311+G*. Our experience has been that diffuse functions generally have little effect on theoretical chemical shifts. However, although the complex is formally neutral, the bonding in MgO is strongly ionic. In addition, we assume that the acetylide dissociates and binds to the surface as $HC{\equiv}C^{\delta-}$ and $H^{\delta+}$. Therefore it is reasonable to assume that diffuse functions may be needed. As Table 8 shows, using 6-311+G* in region 1 reduces the error in the surface-bound C to approximately 1.0 ppm. Unfortunately, the error in the terminal carbon is increased. With 6-311+G* on the atoms in region 1, there is even less sensitivity of the results to the basis sets on more distant atoms. Even when 6-31G is used on all the atoms of Mg_4O_4 there is only a slight deterioration in the agreement for the terminal carbon.

We also completed a similar study using the basis sets of Schafer and Ahlrichs. The Schafer−Alhrichs basis sets used included dzp (O (8s4p1d)/[4s2p1d] and Mg (11s5p)/[6s2p]), tzp (H (5s1p)/[3s1p], C, O (9s5p1d)/[5s3p1d], and Mg (12s9p)/[7s5p]), and tzplarge (H (5s1p)/[3s1p] and C (10s6p1d)/[6s3p1d]). For the tzp and tzplarge basis sets we also added single diffuse s and p functions obtained by even-tempered expansion. We refer to those basis sets as tzp+ and tzplarge+. All the Schafer−Ahlrichs basis sets were used with five d functions. These basis sets have been found to give good results for NMR calculations of a variety of systems. In this case we forego the consideration of a double-ζ basis set on the carbons, instead using only triple-ζ basis sets (tzp, tzp+, or tzplarge+). However, we also divided the cluster into four regions, considering the C and the H separately. With tzp on C, the errors relative to experiment are approximately 2−4 ppm. As was the case for 6-311G* and 6-311+G*, the theoretical values for the C bound to Mg are upfield of experiment, while those of the terminal C are downfield. The results obtained with these basis sets are given in Table 8.

Adding diffuse functions to the C basis sets reduces the error for the Mg-bound C and increases it for the terminal C. Similar behavior was exhibited when we added diffuse functions to the 6-311G* basis set. There is not much difference in the results

(42) Beck, L. W.; Xu, T.; Nicholas, J. B.; Haw, J. F. *J. Am. Chem. Soc.* **1995**, *117*, 11594−11595.
(43) Hariharan, P. C.; Pople, J. A. *Theor. Chim. Acta* **1973**, *28*, 213.
(44) Francl, M. M.; Petro, W. J.; Hehre, W. J.; Binkley, J. S.; Gordon, M. S.; DeFrees, D. J.; Pople, J. A. *J. Chem. Phys.* **1982**, *77*, 3654.
(45) Clark, T.; Chandrasekhar, J.; Spitznagel, G. W.; Shleyer, P. v. R. *J. Comput. Chem.* **1983**, *4*, 294.
(46) Grev, R. S.; Schaefer, H. F., III. *J. Chem. Phys.* **1989**, *91*, 7305−7306.

if we further expand the basis set to tzplarge+. The error for the terminal C decreases by approximately 1.0 ppm. Interestingly, the error when dzp is used on the Mg and O to which the acetylide is bound is much larger when tzplarge+ is used on C than when we use tzp+. Thus, even when a rather large basis set is used on the atoms of interest, there can still be significant effects on accuracy if the basis sets on nearby atoms are inadequate.

We chose to use the Schaefer−Ahlichs basis set for the rest of the NMR calculations presented in this work. Considering the results presented above, we chose to use tzplarge+ on C, tzplarge on H, tzp on the Mg and O associated with the adsorbed species, and dzp on the remaining Mg and O. This scheme affords good accuracy, while allowing us to save computer time through the use of a smaller basis set on the distant atoms. This saving, of course, is more important for the larger MgO clusters. The predicted absolute shielding for C in TMS at this level of theory is 194.4 ppm. To further gauge the expected accuracy of this basis set combination, we also obtained the value for the carbons in gas-phase acetylene. The calculated isotropic chemical shift (adjusted for TMS) is 77.0 ppm. This value is 6.1 ppm downfield of the experimental chemical shift of 70.9 ppm.[48]

Note that, during this analysis, we assumed that the peaks observed experimentally were due to an acetylide and that the Mg_4O_4 cluster would serve as an adequate model of the most active sites. Due to the wealth of data presented earlier, we felt that these were valid assumptions. The fact that the agreement between the theoretical and experimental values becomes better as we make reasonable increases in the basis set size further justifies these assumptions.

JA980384H

(47) Krishan, R.; Binkley, J. S.; Seeger, R.; Pople, J. A. *H. Chem. Phys.* **1980**, *72*, 650.
(48) Jameson, K.; Jameson, C. *Chem. Phys. Lett.* **1987**, *134*, 461−466.